HHS Public Access

Author manuscript

Sci Transl Med. Author manuscript; available in PMC 2020 September 08.

Published in final edited form as:

Sci Transl Med. 2020 April 01; 12(537): . doi:10.1126/scitranslmed.aax6919.

Spontaneous reversal of stenosis in tissue-engineered vascular grafts

Joseph D. Drews[1,2,*], **Victoria K. Pepper**[1,*], **Cameron A. Best**[1,3,*], **Jason M. Szafron**[4,*], **John P. Cheatham**[5], **Andrew R. Yates**[5,6], **Kan N. Hor**[5,6], **Jacob C. Zbinden**[1,7], **Yu-Chun Chang**[1,3], **Gabriel J. M. Mirhaidari**[1,3], **Abhay B. Ramachandra**[4], **Shinka Miyamoto**[1], **Kevin M. Blum**[1,7], **Ekene A. Onwuka**[1,2], **Jason Zakko**[1,2], **John Kelly**[1,5], **Sharon L. Cheatham**[5], **Nakesha King**[1,2], **James W. Reinhardt**[1], **Tadahisa Sugiura**[1], **Hideki Miyachi**[1], **Yuichi Matsuzaki**[1], **Julie Breuer**[1], **Eric D. Heuer**[1], **T. Aaron West**[1], **Toshihiro Shoji**[1], **Darren Berman**[5], **Brian A. Boe**[5], **Jeremy Asnes**[8], **Mark Galantowicz**[5,9], **Goki Matsumura**[10], **Narutoshi Hibino**[11], **Alison L. Marsden**[12], **Jordan S. Pober**[13], **Jay D. Humphrey**[4,*], **Toshiharu Shinoka**[1,5,9,*], **Christopher K. Breuer**[1,2,14,*,†]

[1]Center for Regenerative Medicine, Abigail Wexner Research Institute at Nationwide Children's Hospital, Columbus, OH 43205, USA

[2]Department of Surgery, The Ohio State University Wexner Medical Center, Columbus, OH 43210, USA

[3]Biomedical Sciences Graduate Program, The Ohio State University College of Medicine, Columbus, OH 43210, USA

[4]Department of Biomedical Engineering, Yale University, New Haven, CT 06520, USA

[5]The Heart Center, Nationwide Children's Hospital, Columbus, OH 43205, USA

[6]Department of Pediatrics, The Ohio State University College of Medicine, Columbus, OH 43210, USA

[7]Department of Biomedical Engineering, The Ohio State University, Columbus, OH 43210, USA

[8]Department of Pediatrics, Yale School of Medicine, New Haven, CT 06520, USA

[9]Department of Cardiothoracic Surgery, Nationwide Children's Hospital, Columbus, OH 43205, USA

[†]Corresponding author. christopher.breuer@nationwidechildrens.org.

[*]These authors contributed equally to this work.

Author contributions

J.D.D., V.K.P., C.A.B., J.M.S., J.P.C., A.R.Y., K.N.H., J.D.H., T. Shinoka, and C.K.B. conceived and designed the study. J.D.D., V.K.P., C.A.B., J.M.S., J.C.Z., Y.-C.C., G.J.M.M., A.B.R., S.M., K.M.B., E.A.O., J.Z., J.K., S.L.C., N.K., J.W.R., T. Sugiura, H.M., Y.M., G.M., J.B., E.D.H., T.A.W., T. Shoji, D.B., B.A.B., J.A., N.H., J.P.C., A.R.Y., and K.N.H. acquired the data. J.D.D., V.K.P., C.A.B., J.M.S., J.C.Z., Y.-C.C., G.J.M.M., A.B.R., K.M.B., J.K., J.W.R., A.L.M., M.G., J.S.P., J.P.C., A.R.Y., G.M., K.N.H., J.D.H., T. Shinoka, and C.K.B. analyzed and interpreted the data. J.D.D., V.K.P., C.A.B., J.M.S., J.C.Z., Y.-C.C., G.J.M.M., A.B.R., K.M.B., K.N.H., J.D.H., and C.K.B. drafted the manuscript and figures. All authors critically revised the manuscript and approved the final version and have agreed to be personally accountable for their contributions and to ensure that questions related to the accuracy or integrity of any part of the work, even ones in which the author was not personally involved, are appropriately investigated, resolved, and the resolution documented in the literature.

Data and materials availability

All data associated with this study are present in the paper or the Supplementary Materials.

[10]Department of Cardiovascular Surgery, Tokyo Women's Medical University, Tokyo, Japan

[11]Department of Surgery, University of Chicago/Advocate Children's Hospital, Chicago, IL 60453, USA

[12]Departments of Pediatrics and Bioengineering, Stanford University, Stanford, CA 94304, USA

[13]Department of Immunobiology, Yale University, New Haven, CT 06520, USA

[14]Department of Surgery, Nationwide Children's Hospital, Columbus, OH 43205, USA

Abstract

We developed a tissue-engineered vascular graft (TEVG) for use in children and present results of a U.S. Food and Drug Administration (FDA)–approved clinical trial evaluating this graft in patients with single-ventricle cardiac anomalies. The TEVG was used as a Fontan conduit to connect the inferior vena cava and pulmonary artery, but a high incidence of graft narrowing manifested within the first 6 months, which was treated successfully with angioplasty. To elucidate mechanisms underlying this early stenosis, we used a data-informed, computational model to perform in silico parametric studies of TEVG development. The simulations predicted early stenosis as observed in our clinical trial but suggested further that such narrowing could reverse spontaneously through an inflammation-driven, mechano-mediated mechanism. We tested this unexpected, model-generated hypothesis by implanting TEVGs in an ovine inferior vena cava interposition graft model, which confirmed the prediction that TEVG stenosis resolved spontaneously and was typically well tolerated. These findings have important implications for our translational research because they suggest that angioplasty may be safely avoided in patients with asymptomatic early stenosis, although there will remain a need for appropriate medical monitoring. The simulations further predicted that the degree of reversible narrowing can be mitigated by altering the scaffold design to attenuate early inflammation and increase mechano-sensing by the synthetic cells, thus suggesting a new paradigm for optimizing next-generation TEVGs. We submit that there is considerable translational advantage to combined computational-experimental studies when designing cutting-edge technologies and their clinical management.

INTRODUCTION

Despite advances in surgical management, congenital heart disease remains a leading cause of death in newborns (1, 2). Morbidity and mortality stem, in part, from postoperative complications associated with the synthetic vascular grafts, patches, and replacement heart valves that are used to perform the requisite procedures (3). One considerable limitation of currently available implants is their lack of growth capacity, which can result in somatic overgrowth, including development of relative stenosis as a child outgrows his or her graft (4). Given that somatic overgrowth typically necessitates additional interventions, surgeons attempt to reduce this probability by delaying surgery or oversizing the implant. Yet, these strategies can cause additional problems, including an increased risk for thromboembolic complications, developmental delay secondary to chronic hypoxia, and heart failure due to volume overload (3, 5).

Tissue engineering could reduce complications and enable growth capacity by creating neotissue from an individual's own cells (6). Progress has been made by multiple research groups in the development and translation of tissue-engineered vascular grafts (TEVGs) to the clinic, including conduits for arterial reconstruction, dialysis access, and total cavo-pulmonary connection (7–16). Much of our focus has been on TEVGs for use in congenital heart surgery where the grafts' growth potential can be used to their greatest advantage. Our TEVG is constructed by seeding autologous cells within a porous biodegradable polymeric tubular scaffold (13–14) that provides sites for cell attachment and space for extracellular matrix deposition; neotissue forms as the scaffold degrades, ultimately yielding a polymer-free neovessel. Using this approach, our group conducted a clinical trial in Japan implanting TEVGs in children with single-ventricle cardiac anomalies undergoing congenital heart surgery. These TEVGs demonstrated safety and growth potential, with no acute graft failures or graft-related deaths (14–15). Critical stenosis was observed in 4% (1/25) of patients 3 years after implantation. Given the promising results from this Japanese study, we initiated a clinical trial in the United States to evaluate these TEVGs under the regulation of the U.S. Food and Drug Administration (FDA). This study was placed on hold due to an unexpectedly high incidence of early graft stenosis, although all patients who developed a critical stenosis were successfully treated with angioplasty and completed the 3-year study without additional graft-related complications.

To gain greater understanding of mechanisms responsible for the early TEVG stenosis in the U.S. trial, we first turned to a computational model that we had developed to simulate neovessel formation in an inferior vena cava (IVC) interposition TEVG model. This computational model had successfully described and predicted neovessel formation over a 2-year period in mice (17–19). Here, we present new computational results that suggest that the early stenosis observed in our U.S. trial may have spontaneously reversed without intervention, a reversal that may have existed in the Japanese trial but went undetected because of the lack of consistent, early medical imaging. We then present experimental results from an ovine IVC interposition TEVG model that confirm the unexpected simulation-generated hypothesis that graft narrowing can resolve as part of the natural progression of neovessel formation. Ovine data on the evolving composition and biomechanical properties of these TEVGs were also consistent with predictions of the computational model, which provides increased insight into sequential mechanisms that underlie the transformation of TEVGs from cell-seeded polymeric scaffolds into living neovessels having growth capacity. This computational-experimental paradigm has important implications for the design of future clinical studies evaluating TEVGs as well as development of new strategies for improving the design of scaffolds to optimize graft performance.

RESULTS

Clinical trial

The goal of the FDA-approved clinical trial (IDE 14127) was to use a stringent protocol, including frequent imaging over a 3-year period, to determine the incidence of graft-related complications (safety) of TEVGs used in an extracardiac modified Fontan operation to

connect the IVC to the pulmonary artery in children with single-ventricle cardiac anomalies. The clinical trial flow chart and summary, as well as patient demographics, are included in the Supplementary Materials (fig. S1 and table S1).

Design and characterization of the TEVG

TEVGs used in the clinical trial were assembled by seeding autologous bone marrow–derived mononuclear cells onto a biodegradable tubular scaffold (13). The scaffolds (Gunze Ltd.) were made from poly(glycolic acid) (PGA) fibers and a copolymer of caprolactone and lactide (PCLA); they were designed to degrade by hydrolysis over 6 months (13). Scaffolds measured either 16 ± 0.5 mm or 18 ± 0.5 mm in inner diameter, 13 ± 0.5 cm in length, and 0.7 ± 0.1 mm in wall thickness (Fig. 1A). Quantitative scanning electron microscopy of the inner surface revealed an average pore size of 41.9 ± 2.7 μm and porosity of 0.87 ± 0.01; average pore size was 36.4 ± 6.6 μm, and porosity was 0.86 ± 0.02 on the outer surface. Average PGA fiber diameter was 15.8 ± 1.0 μm (Fig. 1B).

In the clinical trial, TEVGs were assembled in compliance with Good Manufacturing Practice (GMP) regulations. Bone marrow (5 ml/kg body weight) was harvested from the patient on the day of surgery, and the mononuclear cell fraction was separated using density centrifugation in Ficoll (13). This procedure yielded an average of 3.4×10^8 mononuclear cells (range, 2.2 to 4.9×10^8 cells) with an average cell viability of 92.6% (range, 86.5 to 96.8%). Flow cytometry demonstrated that 78.3% (range, 73.2 to 85.3%) of these cells were $CD45^+$. These cells were seeded onto the polymeric scaffold using a custom vacuum system, which yielded an average seeding efficiency of 42.7% (range, 23 to 61.4%). The seeded scaffold was incubated in autologous plasma for 2 hours before implantation, on the same day the TEVG was assembled (Fig. 1C). All TEVGs met the release and postprocess monitoring criteria (table S2).

TEVG performance in the U.S. trial

Safety analyses demonstrated no graft-related deaths, catastrophic graft failures, or complications requiring graft replacement during the 3-year study. However, three of the four patients developed critical TEVG stenosis (defined as stenosis requiring angioplasty) and were successfully treated with angioplasty 5 to 8 months after implantation (Fig. 2, A to C). There were no additional graft-related complications. Indications for angioplasty included a >50% reduction in luminal diameter and an associated pressure gradient >0.5 mmHg. The individual pre- and post-angioplasty images, including morphometric and hemodynamic assessment, are included in the Supplementary Materials (fig. S2). Enrolment was capped at 4 patients instead of the intended 6, because of this unexpectedly high incidence of critical TEVG stenosis (75%), recalling that only 1 of 25 patients (4%) in the original Japanese trial developed stenosis requiring angioplasty within 3 years after implantation (two-sided Fisher's exact test, $P < 0.01$) (14, 15).

Computational model of neovessel development

Our computational model delineates immuno-driven and mechano-mediated neotissue production and removal within a degrading polymeric scaffold (Fig. 3A) while enforcing mechanical equilibrium within each of the evolving states. The theoretical framework and

modeling background are summarized in the Supplementary Materials (table S3). Our previous studies of IVC interposition TEVGs in immunocompetent and immunocompromised mice revealed similar mechano- but different immuno-stimulated extracellular matrix turnover in these two mouse models (19), the latter governed by four key parameters (Fig. 3B): δ modulates the onset and duration of the inflammatory response; β controls the skewness of the inflammatory matrix production profile; K_h^i controls rates of inflammatory matrix production and degradation; and K_{max}^i scales the inflammatory effects of matrix degradation, all over time τ, with the overall rate of inflammatory matrix production given by

$$m^i(\tau) = m_h^i(1 - \exp(-\tau))K^i\Gamma^i(\tau)$$

where m_h^i is the basal rate of production of matrix constituent *i* driven by inflammation and $K^i = K_h^i(r_p/r_n) + K_w^i$ is the gain for a gamma function $\Gamma^i(\tau) = \Gamma(\tau)/\max(\Gamma(\tau))$, with $\Gamma(\tau) = \delta^\beta\tau^{\beta-1}\exp(-\delta\tau)$, that describes the onset and resolution of the foreign body response to the degrading polymer, with r_p/r_n the pore size of the scaffold normalized by a critical pore size for cellular infiltration and K_w^i a basal gain for inflammation-driven matrix production. Degradation of the inflammatory matrix is governed by a first-order type kinetic decay (Fig. 3A),

$$q^i(s,\tau) = \exp\left(-\int_\tau^s k_h^i\left(1 + K^i/K_{max}^i\right)dt\right)$$

where k_h^i is a rate parameter and K_{max}^i is the maximum value of K^i (*2–21*). Descriptions of the mechanical properties of the different constituents and values of the other model parameters are in the Supplementary Materials (fig. S3 and table S4).

Parametric simulations of neotissue formation

We first used the computational model to predict the evolving normalized luminal diameter and wall thickness of a TEVG using values of the model parameters determined by fitting longitudinal morphological and biomechanical data from previous mouse experiments but with appropriate scaling of geometric (diameter/thickness ratio, $D/H = 16$ for the clinical scaffold versus $D/H = 3$ for the mouse scaffold) and microstructural (scaffold pore size, r_p = 41.9 μm for clinical scaffold versus 11.2 μm for mouse scaffold) properties to account for differences between the clinical and mouse scaffolds. Because the inflammation-driven kinetics were known for the murine data and the immune response plays a critical role in stenosis, parametric studies were performed for the four key inflammatory parameters (δ, β, K_h^i, and K_{max}^i) by varying the value of an individual parameter while holding constant the other three and vice versa. This allowed us to isolate effects of each parameter on the evolving TEVG properties, including diameter (Fig. 3, C to F) and wall thickness (Fig. 3, G to J), which were normalized by nominal values for the implanted TEVG scaffold.

Corresponding profiles of both immuno-mediated and mechano-mediated matrix formation for these geometric time courses are shown in the Supplementary Materials (figs. S4 to S6).

Myriad simulations of neovessel development allowed us to accomplish something not possible with in vivo studies—to isolate effects of individual contributors to the evolution of key TEVG properties over the desired time course. The depicted parameter ranges (Fig. 3B) captured a wide range of potential physiologic outcomes based on broader preliminary studies (figs. S4 to S6). These simulations predicted findings similar to those observed in our U.S. clinical trial, namely, an early narrowing of the TEVG, but they suggested further that this narrowing resulted from a marked inflammation-driven neotissue thickening of the wall. Unexpectedly, however, the model also predicted that such narrowing could spontaneously reverse in a broad range of cases (Fig. 3, C to J) as the immune response waned with polymer degradation and subsequent mechano-mediated neotissue degradation outpaced deposition as wall stress dropped well below normal homeostatic values due to both narrowing and thickening. We had not previously considered the possibility that TEVG stenosis could spontaneously reverse. The computational model thus generated an unexpected hypothesis that we then tested experimentally using an ovine model.

TEVG stenosis reverses spontaneously in a large animal model

To test our computational model predictions, we used a juvenile ovine intrathoracic IVC interposition graft model, a surrogate for the modified Fontan operation (22–24). The ovine study design, surgical outcomes, and animal tracking data are included in the Supplementary Materials (fig. S7 and table S5). The TEVGs were made with the same scaffolds used in the clinical trial and were assembled using the same methodology except that cell isolation and seeding were not performed in compliance with GMP standards. In the ovine study, bone marrow (5 ml/kg body weight) yielded an average of 1.4×10^{10} cells (range, 4.6×10^{8} to 4.5×10^{10}) with an average viability of 96.8% (range, 91.8 to 100%). The average seeding efficiency was 37.8% (range, 10.3 to 88.4%).

We implanted size-matched TEVGs into 24 lambs, 22 of which survived the perioperative period. TEVG morphology was serially monitored using angiography and intravascular ultrasound (IVUS), including luminal diameter, cross-sectional area, and wall thickness over 1 year (fig. S8, A to D). Angiography revealed significant TEVG stenosis at 6 weeks [−0.64 ± 0.10–fold diameter change from 1-week midgraft; one-way analysis of variance (ANOVA) with repeated measures followed by Tukey's multiple comparisons test: $\alpha = 0.05$, $P < 0.001$]. Yet, as predicted by the model, the stenosis improved spontaneously without endovascular intervention, and all TEVGs remained patent throughout the course of the study (fig. S8B).

IVUS suggested that the early TEVG narrowing resulted from appositional growth of neotissue on the luminal surface of the scaffold, thus thickening the wall and narrowing the lumen. At 6 weeks, the TEVG stenosis was localized to the mid-distal segment of the graft (the region closer to the heart), whereas no changes were identified at the proximal anastomosis. Quantitative IVUS confirmed that the luminal area decreased significantly from 1 to 6 weeks (−0.76- ± 0.12-fold area change from 1-week midgraft area: $\alpha = 0.05$, $P < 0.001$) and that the narrowing reversed by 6 months, with the grafts remaining patent at 1

year (fig. S8C). During this same period, the wall reached its maximum thickness at 6 weeks (range, 2.9 to 6.2 mm: $\alpha = 0.05$, $P < 0.001$) and then thinned progressively over the 1-year time course (fig. S8D).

We also collected hemodynamic data during each cardiac catheterization. The mean pressure gradient across the graft followed the aforementioned morphometric changes. The gradient increased significantly from 1 to 6 weeks (0.5 ± 0.5 versus 11.8 ± 5.5 mmHg: $\alpha = 0.05$, $P < 0.001$) and then decreased to near baseline by 6 months (1.3 ± 2.8 mmHg: $\alpha = 0.05$, $P < 0.001$ versus 6 weeks, $P = 0.61$ versus 1 week) (fig. S8E). The largest pressure gradients tended to correspond to the narrowest grafts (fig. S8F). Two animals (9.1% of those who survived the perioperative period) developed symptoms including ascites, lethargy, and weight loss. Both of these lambs had mean pressure gradients >19 mmHg at 6 weeks, and their grafts were two of the three narrowest as determined using angiography, measuring less than 4 mm luminal diameter at the narrowest point. These two symptomatic animals were euthanized. Despite marked TEVG narrowing in the remaining animals, they remained asymptomatic and their stenosis resolved spontaneously. None of the grafts occluded acutely, and no animals died as a result of stenosis. A table summarizing the individual results of the ovine cardiac catheterizations, including morphometric and hemodynamic assessments, is in the Supplementary Materials (table S6).

Computational model validation

Whereas our hypothesis-generating simulations were parameterized on the basis of studies of an IVC interposition TEVG in mice that consisted of a scaffold similar to that of the ovine and clinical grafts (Fig. 3, B and C), we sought to determine whether our model could also describe the in vivo ovine data. When informed with parameters from the murine studies, the model captured the time course of the narrowing and wall thickening followed by spontaneous reversal in the lambs, though suggesting a milder phenotype (fig. S9). We thus determined best-fit values of the four key inflammatory parameters (Fig. 3B) based on hydraulic diameter measurements from the ovine IVUS data, normalized to the original implantation dimensions of the scaffold (finding, $\delta = 0.32$ days^{-1}, $\beta = 4.00$, $K_h^i = 4.89$,and $K_{max}^i = 76$), which enabled the model to fit the morphological data well ($R^2 = 0.80$) at all times (Fig. 4), despite retaining many parameter values from the murine experiments (mechanical properties and basal rates of turnover for collagen; tables S4 and S7).

Evolving neovessel composition and mechanics are consistent with computational predictions

We also characterized longitudinal changes in the ovine neotissue using histology and immunohistochemistry. Histological sections confirmed changes in the lumen and wall thickness of the TEVGs that were observed with in vivo imaging and verified that the transient luminal narrowing was primarily due to wall thickening with some excessive neotissue formation on the luminal surface that appeared to resolve by 6 months after implantation (Fig. 5A). Quantitative histomorphometry demonstrated that measured wall thickness peaked 6 weeks after implantation (Fig. 5B), consistent with the computational predictions (Fig. 5C). Immunohistochemical staining for α-smooth muscle actin (αSMA) identified cells along the luminal surface of the scaffold as well as within the scaffold; their

number was also greatest at 6 weeks. The αSMA^+ cells along the luminal surface were presumed to be smooth muscle cells that proliferated and contributed to the neotissue that caused TEVG stenosis (Fig. 5D). The overall number of αSMA^+ cells peaked early, which fit well with the observed (Fig. 5E) and model-predicted (Fig. 5F) early exuberant production of matrix. The degree of macrophage infiltration was assessed using immunohistochemical staining against CD68 (Fig. 5G), which revealed the greatest macrophage density at 6 weeks. Beyond 6 months, the number of macrophages diminished consistent with scaffold degradation (Fig. 5H), which also aligned with the computational predictions of the inflammatory time course (Fig. 5I). Thus, the model suggestion that TEVG stenosis is largely inflammation-driven was supported by the in vivo ovine data. An expanded histological and immunohistochemical evaluation of the longitudinal changes in the ovine neotissue is included in the Supplementary Materials (fig. S10).

The sum of the mechanical contributions of the polymeric scaffold and neotissue (determined primarily by the extracellular matrix component) determines the bulk properties of the TEVG. We characterized scaffold degradation and neotissue formation using polarized light images of Picro-Sirius Red (PSR)–stained sections from ovine TEVGs obtained 1 week, 6 weeks, 6 months, and 1 year after implantation, which revealed both the degradation of PGA fibers and deposition and maturation of collagen fibers (Fig. 6A). The PGA fibers remained highly organized within the scaffold 1 week after implantation but had thinned and begun to fragment at 6 weeks. Only rare, thin, individual fragments of the PGA fibers were visible 6 months after implantation and beyond. In contrast, minimal staining was detected for fibrillar collagen at 1 week. Total collagen in the neotissue peaked 6 weeks after implantation, with considerable thin (green) fibers within the scaffold and along its luminal surface. Collagen density increased steadily over the first year as it compacted and matured (Fig. 6, B and C). This collagen appeared to be the primary extracellular matrix component of the neotissue associated with TEVG stenosis, as assumed in the model. The collagen also appeared to remodel between 6 weeks and 6 months, as the scaffold degraded and the wall thinned; at 6 months, collagen fibers appeared orange, signifying that they were of medium thickness. One year after implantation, the wall had become even thinner and the collagen fibers appeared thicker (red) and denser, suggestive of normal, mature vascular collagen.

In vitro biaxial mechanical testing of TEVGs excised at the 1.5-year end point revealed a structural response (pressure diameter) of the TEVG similar to model predictions (Fig. 6D). The final compliance of the TEVG, which was predicted by the computational model as a validation step rather than based on a fit to data, also matched well with values found from the ex vivo mechanical characterizations at 1.5 years (Fig. 6E). Values of the material parameters in the computational model suggested that this bulk behavior resulted from a higher inflammation-driven matrix turnover than mechano-mediated matrix turnover throughout much of neovessel development (fig. S6), as the mechanical stimuli for neotissue production were attenuated by the high wall thickness and low diameter.

Re-evaluation of the clinical trials

Retrospective review of the indications for angioplasty in the U.S. trial demonstrates that only one of the four (25%) angioplasties performed met the Japanese criteria (fig. S11). This is an important distinction because in the FDA-approved trial, the need for angioplasty defined a serious graft-related complication, whereas stenosis not treated with angioplasty was considered a nonserious graft-related complication. Ultimately, it was the higher-than-predicted incidence of critical stenosis (requiring angioplasty) that led to the premature closure of the U.S. trial. Our identification of the reversible nature of early TEVG stenosis calls into question this interventional strategy.

Patients in the U.S. underwent, on average, 15 echocardiograms and one magnetic resonance imaging (MRI) during the first year after surgery, whereas patients in Japan underwent an average of two imaging studies (14), the first within 1 month after implantation and the second up to a year after implantation (fig. S12). Note, therefore, that most cases of TEVG stenosis in the U.S. clinical trial and ovine study were asymptomatic and would not have been detected without frequent imaging. We contend, therefore, that patients in the Japanese trial could have developed silent stenosis that was not detected or was detected in a delayed fashion. Although review of data from the Japanese cohort is partially limited because of the heterogeneity of the imaging modality and timing of the imaging studies and because many of the images were not archived, retrospective analysis of available images revealed that at least one patient who would have met the U.S. criteria for angioplasty, but instead was serially monitored, had reversal of TEVG narrowing without intervention (fig. S13). An additional patient, one of the two patients in the Japanese trial to develop a critical graft-related complication during the first 3 years after implantation, underwent catheterization 11 months postoperatively that revealed stenosis with no pressure gradient. A follow-up computed tomographic (CT) scan 2 weeks later demonstrated TEVG wall thickening causing luminal narrowing; this was interpreted to represent a mural thrombus. The patient was started on oral anticoagulation therapy and serially monitored with CT scans over the ensuing 3 years, during which the narrowing reversed; however, CT imaging cannot distinguish mural thrombus from neotissue in a TEVG. In light of the absence of any other thrombotic complications in either clinical trial, as well as absence of TEVG thrombosis in our lamb study, it is intriguing to surmise that this may have represented the first documented, though unrecognized, case of reversible TEVG stenosis reported in the literature (Fig. 7) (15).

DISCUSSION

To gain mechanistic insight into the complex immunobiological and mechanobiological processes that could have caused early TEVG stenosis in our U.S. trial, we used a computational model of neovessel development to study parametrically the relative contributions of multiple critical factors that control neotissue formation. This model predicted not only early graft narrowing but also spontaneous reversal, an unexpected finding that was reproducibly confirmed in an ovine IVC interposition graft model. These findings suggest that we may have over-treated the patients in our FDA-approved clinical trial with early angioplasty. Asymptomatic TEVG stenosis was safely monitored in the

lambs over the entire study period, without any acute graft failures or thrombosis. Given that the two lambs with symptomatic stenosis were euthanized per protocol, we do not know whether those animals could have been salvaged with angioplasty once the symptomatic stenosis developed or whether intervention would have been needed before development of clinical signs. Regardless, this study uncovered a distinct natural history of a class of TEVGs and emphasizes that we should avoid biases based on experience with native tissues and pathologies.

In retrospect, premature closure of the U.S. trial due to the unexpected high incidence of early stenosis may have been avoided if the spontaneous reversal of TEVG stenosis had been appreciated. A major reason for the high incidence of early critical stenosis in the U.S. trial versus the Japanese trial arose due to differences in criteria for performing angioplasty. In the U.S., the interventional cardiologist adopted a more aggressive approach wherein angioplasty was based primarily on graft morphometry, whereas in Japan the interventional cardiologists adopted a more conservative approach, performing angioplasty based on hemodynamic metrics. Specifically, in the U.S., patients with >50% reduction in graft diameter relative to the nominal graft size with any pressure gradient (>0.5 mmHg) underwent angioplasty. In Japan, a 50% reduction in graft diameter was used as an indication for angiography, but only patients with pressure gradients of at least 2 mmHg along the graft or 1 mmHg along the graft with evidence of collateral formation underwent intervention, independent of graft diameter.

As TEVGs continue to advance to the clinic, TEVG-specific indications for angioplasty may need to be developed anew because reversible stenosis is a new condition. Of course, the findings from our animal study should inform, but will likely not directly translate to, clinical decisions, particularly because consequences of not treating a stenosis in a timely manner could be critical for children receiving our graft. Thus, on the basis of findings currently available, the presence of symptoms or the development of narrowing with a pressure gradient >2 mmHg may serve as the primary criteria in assessing the clinical significance of TEVG stenosis rather than morphometric changes alone. Although adopting a more conservative interventional approach could simply delay the need for treatment, our findings suggest that many cases of early stenosis may naturally resolve; hence, appropriately frequent monitoring rather than overly aggressive intervention appears to be a way forward.

Collectively, results from our previous murine studies coupled with our human clinical trials, computational simulations, and ovine studies suggest that implantation of a cell-seeded PGA/PCLA scaffold as a TEVG sets into motion an inflammation-driven, mechano-mediated remodeling process that converts a polymeric scaffold into a living neovessel. The polymer initially incites a strong foreign body response, and host inflammatory cells infiltrate the scaffold. Simultaneously, the scaffold partially shields the infiltrating vascular cells, and the neotissue they deposit, from the hemodynamically imposed mechanical loads until the structural integrity of the polymer is lost. Mechanobiological processes thus appear to increase as scaffold integrity diminishes, and low wall stresses due to early over-thickening of the graft cause matrix degradation to initially outpace deposition, resulting in a progressive resolution of the initial inflammation-driven stenosis. The inflammation is not

completely detrimental, however; some inflammation is fundamental to early host cell recruitment and neotissue formation (25–27). Infiltrating monocytes/macrophages orchestrate early neotissue formation by inducing ingrowth of host endothelial and smooth muscle cells from the neighboring vessel wall (28). Overall TEVG functionality thus requires a balanced degradation of the polymeric scaffold and appropriate deposition of neotissue (by synthetic cells, with strong paracrine effects). Going forward, it appears that it will be critical to promote, but limit, inflammation while simultaneously optimizing the timing of load transferal from the degrading polymeric scaffold to the cell-matrix composite that constitutes the neotissue (fig. S14). In previous preclinical studies, we have examined a variety of strategies for inhibiting inflammation-mediated TEVG stenosis (29–33), including inhibition of transforming growth factor–β receptor 1 (TGFβR1), administration of cilostazol or losartan, and altering the number of seeded bone marrow–derived mononuclear cells. When and how to implement these strategies demand further study. What effect these strategies will have on early or late neotissue formation in patients remains to be seen and warrants active investigation.

Albeit very encouraging, this work is not without limitations. With regard to the computational model, we emphasize that one must first think of limitations in terms of goals, not absolutes. Our initial goal was to describe and predict the transformation of an implanted polymeric scaffold into a living neovessel, specifically within the context of a size-matched interposition IVC graft. Hence, the hemodynamics were expected to be well described by a Poiseuille solution, thus avoiding limitations such as assumptions of no flow or inviscid flow. Moreover, the wall mechanics were expected to manifest in a nearly straight, uniform thickness tube as described by the Laplace solution, which is exact and universal (independent of constitutive assumptions) for mean wall stress, thus avoiding limitations such as an assumption of linearized elasticity. As we note above, the model included complexities that were critical, such as the different nonlinear material properties and rates of turnover of immuno- and mechano-mediated neotissue as well as separate polymer properties and degradation. The model was informed by data and able to describe and predict murine and ovine data well, with unexpected predictions that motivated subsequent experiments that confirmed the predictions. That said, our present model will need to be modified as we move forward and seek to address additional goals, which is now justified given our past successes. In this spirit, to move toward a full description of the spatiotemporal changes that characterize the clinical situation, we will need to extend the model to account for evolving asymmetric geometries with axial and radial variations, and we will need to couple a full, three-dimensional hemodynamic simulation to the growth and remodeling simulation.

Because we have observed patient-specific differences in outcomes, we will also need to determine whether (and which) patient-specific data such as preoperative imaging, pre- and postoperative molecular imaging, or pre- and postoperative biomarkers can be used to inform the model further to predict specific natural histories. The natural history of possible stenosis beyond the early period (1 to 3 years postoperatively) also remains unclear because it was not considered computationally or evaluated in the ovine model. The lamb intrathoracic interposition graft model is limited as well, yet there are currently no single-ventricle cardiac anomaly models for preclinical investigations, and performance of a Fontan

operation on an animal with a normal heart associates with prohibitively high postoperative mortality. It was for these reasons that we developed the intrathoracic IVC interposition graft model to serve as a surrogate for the Fontan operation. Because the juvenile ovine size and anatomical structures are similar to those of children undergoing Fontan surgery and because the flow through the conduit is similar, we contend that this model is relevant for evaluating TEVG performance, particularly because it mimics the clinical performance of the TEVG in that stenosis is the most common graft-related complication. FDA approval of our clinical trial was based, in part, on this ovine model. Although species-specific phenomena are always a possibility, retrospective review of our Japanese data suggests that this was not a major issue. The two main differences between the ovine model and the clinical study pertain to the time course and the hemodynamic pressures, not the primary outcomes. The stenosis peaked around 6 weeks after TEVG implantation in our ovine study, whereas this typically occurred around 5 to 6 months after implantation in the clinical trial. Although the flow through the TEVG in the ovine model is similar to the flow through the TEVG in the clinical studies, the pressures are typically much less. Moreover, much higher pressure gradients (up to 20 mmHg) are tolerated in the IVC interposition graft model than in the Fontan circulation, where pressure gradients as low as 2 mmHg cause symptoms. These differences make direct comparison between the ovine and human studies challenging. Our computational model-generated prediction of reversible stenosis was validated using the ovine model, but additional clinical work will be needed to determine the optimal timing and indications for performing TEVG angioplasty.

Much can be learned across the many different studies of TEVGs in the scientific literature. Multiple groups have reported critically important work that has advanced TEVGs toward the clinic, though mainly for different clinical targets. Most TEVGs are designed for the arterial circulation, including small-vessel TEVGs used as vascular bypasses or arteriovenous grafts (34–7). These TEVGs differ from the large-diameter venous grafts in this study and typically suffer different complications (aneurysmal dilation or thrombosis, not stenosis). Other groups also use different materials and fabrication methods (37–43). The unseeded, bioabsorbable supramolecular polymer TEVG manufactured by Xeltis is probably most comparable to our graft; it has been implanted as an extracardiac conduit in five patients undergoing modified Fontan procedures in Russia (16). No graft-related complications occurred within a 1-year follow-up, but the Xeltis scaffold degrades over a much longer period than 1 year. There is a need to evaluate safety, efficacy, and growth potential well after the polymer disappears to ensure safety and confirm efficacy (44). To date, there have also been multiple uses of computational models to advance TEVG design. Models have been used to better prescribe the mechanical properties of electrospun grafts at the time of implant (45–46), a general approach reviewed in (47), as well as to predict neovessel development ex vivo in bioreactors (48). Both agent-based (49) and constrained mixture (50) models have been used for such modeling. In contrast, we focused on the in vivo development of a neovessel, accounting for immuno- and mechano-stimuli, with the former depending on microstructural features of the scaffold. Our approach thus provides a general framework for analyzing many TEVGs, given appropriate data. In addition to predicting graft performance, it can also be used as a tool in the development and optimization of TEVGs (51). Nevertheless, differences in tissue engineering methodology as

well as potential differences in mechanism of action limit the generalizability of our current findings to other TEVGs. The computational model was tuned for our graft, and the clinical and preclinical results described here may be different for different grafts. Additional experimentally derived data will be needed to inform the model before it can be applied to other types of TEVGs.

In conclusion, this study further demonstrates the utility of combining advanced computational modeling and model-driven preclinical experiments in translational research. A similar approach has been shown to advance tissue-engineered heart valve design (52). Our framework is distinct, however, given that the simulations predict changes in geometry, composition, and biomechanics of an evolving TEVG that result from immunobiological and mechanobiological stimuli. Results suggest that at least some of the early stenosis observed in our clinical trial, which resulted in our study closing prematurely, may have resolved spontaneously without angioplasty. Early asymptomatic TEVG narrowing appears to be a well-tolerated part of the natural history of neovessel formation, thus providing support for redesigning and reinitiating our clinical trial using less aggressive angioplasty criteria coupled with cautious monitoring of patient physiology and graft morphometry. Last, the computational simulations also suggest that it should be possible to reduce the degree and duration of narrowing by altering the scaffold design to alter the associated inflammation and mechanical stress shielding. In this way, the proposed computational-experimental approach promises both to guide clinical usage of a new technology and to accelerate the iterative design process for improving next-generation designs via early in silico studies that reduce the experimental search space. In this context, recently proposed optimization methods may provide a valuable means to identify new candidate designs (53). Computational models can thus help accelerate the process of safely translating cardiovascular tissue engineering technologies to the clinic, demonstrated here with the goal of improving surgical outcomes in children born with congenital heart disease.

MATERIALS AND METHODS

Study design

Clinical trial—The primary objective of this pilot trial was to evaluate the safety of TEVGs as extracardiac modified Fontan conduits in patients with single-ventricle cardiac anomalies. The original design was to enroll six patients and monitor them with serial echocardiography and MRI over a 3-year period. Upon completion of the study, all patients were to be enrolled in a long-term observational study to evaluate late-term graft performance. The clinical trial flow chart and summary are in the Supplementary Materials (fig. S1). Additional information on clinical methods and materials is also in the Supplementary Materials. Institutional review board (IRB) approval was granted by Yale University (Human Investigation Committee #0701002198) and Nationwide Children's Hospital (IRB12–00357 and IRB15–00013). The clinical trial was performed under FDA IDE 14127 in compliance with good clinical practice guidelines.

Computational modeling study—We extended a previously developed computational model of TEVG growth and remodeling (17–19, 54) to gain further insight into an

unexpected finding in the clinical trial, namely, early stenosis. An initial computational study was designed to use extensive parametric studies to explore potential mechanisms of remodeling of a generic TEVG based on data from previous murine studies of IVC interposition TEVGs implanted over long periods. On the basis of these computational results, we then designed follow-up simulations to evaluate model predictions using data from long-term studies of IVC interposition TEVGs in lambs, particularly the prediction that immuno-driven and mechano-mediated mechanisms (20–21, 55–56) drive a spontaneous reversal of stenosis in TEVGs in vivo. Further details on model development and usage are in the Supplementary Materials (see also figs. S6 to S9 and S12; tables S3, S4, S7, and S8; and data file S1).

Ovine study—The objective of this study was to test the unexpected computationally generated hypothesis by quantifying the natural history of neotissue formation and thus neovessel development more than 1 year in a lamb IVC interposition model (22–24). Seeded TEVGs were implanted in 24 lambs, and in vivo data were collected via serial angiography and IVUS at 1 week, 6 weeks, 6 months, and 1 year. One week was used for baseline anatomic information; it not only provides comparable data to the immediate postoperative period but also allows the animal to recover from the initial surgical insult and decreases risks associated with the prolonged anesthesia needed to perform the implantation surgery and an initial catheterization during the same period. Additional details are in the Supplementary Materials (see also figs. S10 to S13 and tables S7 and S8). The Institutional Animal Care and Use Committee of Nationwide Children's Hospital (Columbus, OH) reviewed and approved the protocol for the ovine study (AR13–00079). Representatives of the animal care staff monitored all animals intraoperatively and during their postoperative courses. Animal care was within the humane guidelines published by the Public Health Service, National Institutes of Health (Bethesda, MD) in the care and use of laboratory animals (2011), as well as within U.S. Department of Agriculture regulations set forth in the Animal Welfare Act.

Statistical analysis

Statistical analyses were performed, and graphs were created using GraphPad Prism version 7.03 (GraphPad Software Inc.). The incidence of early stenosis in the Japanese versus U.S. clinical trials was compared using a two-tailed Fisher's exact test. Serial measurements from the ovine study (angiography and IVUS) were first normalized to paired 1-week values to control for variable scaffold sizes used at implantation to ensure size matching to the native vessel or variable degrees of anastomotic narrowing as a result of the implantation procedure and are thus represented as a fold change relative to the respective 1-week measurement. Pressure measurements or normalized angiographic and IVUS values were analyzed using a one-way ANOVA with repeated measures followed by Tukey's post hoc multiple comparisons test. Histomorphometric and micrographic data (wall thickness, αSMA^+ area fraction, $CD68^+$ cells/mm^2, and collagen area fraction) were analyzed via one-way ANOVA with Tukey's post hoc multiple comparisons test. For all statistical tests, α was restricted to 0.05 and $P < 0.05$ was considered statistically significant. Primary data are reported in data file S2.

Supplementary Material

Refer to Web version on PubMed Central for supplementary material.

Acknowledgments

We thank our Data Safety Monitoring Board (R. Shaddy, G. Wernovsky, R. Burke, D. Mooney, and J. Burns), the Nationwide Children's Hospital Animal Research Core (H. Pisharath, L. Goodchild, A. Morrison, A. Artrip, A. Ashbrook, K. Nelson, J. Hamilton, and C. Haller), Interventional Cardiology staff (J. Chisolm, A. Latham, J. Swinning, P. Lawrence, and A. Harrison), and A. Lee for their assistance completing the work described here.

Funding: This research was supported by U.S. NIH grants: R01HL098228, R01HL128602, R01HL128847, and R01HL139996, in addition to the Department of Defense Application ID PR170976 Award Number W81XWH-18-1-0518. Funding was also provided by the NIH (TL1TR001069 to J.D.D. from the National Center for Advancing Translational Sciences; 2T32GM068412-11A1 to C.A.B. from the National Institute of General Medical Sciences; T32AI106704 to E.A.O. and TL1TR002735 to J.Z. from the National Center for Advancing Translational Sciences; Diversity Supplement Grant 3R01HL098228-06S1 to N.K.; T32HL098039-06A1 to J.W.R. and T32HL098039 to J.K. from the National Heart, Lung, and Blood Institute). J.M.S. was supported by NSF Graduate Research Fellowship DGE1122492. J.W.R. was supported, in part, by the American Heart Association under Award Number 18POST33990231.

Competing interests

C.K.B. is an inventor on patent/patent applications [2015252805 (Australia), 2016565483 (Japan), 855,370, 9,446,175, 9,782,522, 10,300,082, 61/987,910, 62/266,309, 62/309,285, 62/209,990, 62/936,225] submitted by Yale University and/or Nationwide Children's Hospital that cover methods of improving the design, manufacturing, or performance of tissue-engineered vascular grafts. C.K.B. is a founder of Lyst Therapeutics. C.K.B. and T. Shi have received grant support from Gunze Ltd., and Gunze Ltd. provided support for the clinical trial.

REFERENCES AND NOTES

1. van der Linde D, Konings EEM, Slager MA, Witsenburg M, Helbing WA, Takkenberg JJM, Roos-Hesselink JW, Birth prevalence of congenital heart disease worldwide: A systematic review and meta-analysis. J. Am. Coll. Cardiol. 58, 2241–2247 (2011). [PubMed: 22078432]
2. Simeone RM, Oster ME, Cassell CH, Armour BS, Gray DT, Honein MA, Pediatric inpatient hospital resource use for congenital heart defects. Birth Defects Res. 100, 934–943 (2014).
3. Drews JD, Miyachi H, Shinoka T, Tissue-engineered vascular grafts for congenital cardiac disease: Clinical experience and current status. Trends Cardiovasc. Med. 27, 521–531 (2017). [PubMed: 28754230]
4. Shinoka T, What is the best material for extracardiac Fontan operation. J. Thorac. Cardiovasc. Surg. 153, 1551–1552 (2017). [PubMed: 28314526]
5. Alexi-Meskishvili V, Ovroutski S, Ewert P, Dähnert I, Berger F, Lange PE, Hetzer R, Optimal conduit size for extracardiac Fontan operation. Eur. J. Cardiothorac. Surg. 18, 690–695 (2000). [PubMed: 11113677]
6. Langer R, Vacanti JP, Tissue engineering. Science 260, 920–926 (1993). [PubMed: 8493529]
7. L'Heureux N, McAllister TN, de la Fuente LM, Tissue-engineered blood vessel for adult arterial revascularization. N. Engl. J. Med. 357, 1451–1453 (2007). [PubMed: 17914054]
8. Kirkton RD, Santiago-Maysonet M, Lawson JH, Tente WE, Dahl SLM, Niklason LE, Prichard HL, Bioengineered human acellular vessels recellularize and evolve into living blood vessels after human implantation. Sci. Transl. Med. 11, eaau6934 (2019). [PubMed: 30918113]
9. McAllister TN, Maruszewski M, Garrido SA, Wystrychowski W, Dusserre N, Marini A, Zagalski K, Fiorillo A, Avila H, Manglano X, Antonelli J, Kocher A, Zembala M, Cierpka L, de la Fuente LM, L'Heureux N, Effectiveness of haemodialysis access with an autologous tissue-engineered vascular graft: A multicentre cohort study. Lancet 373, 1440–1446 (2009). [PubMed: 19394535]
10. Lawson JH, Glickman MH, Ilzecki M, Jakimowicz T, Jaroszynski A, Peden EK, Pilgrim AJ, Prichard HL, Guziewicz M, Przywara S, Szmidt J, Turek J, Witkiewicz W, Zapotoczny N, Zubilewicz T, Niklason LE, Bioengineered human acellular vessels for dialysis access in patients

with end-stage renal disease: Two phase 2 single-arm trials. Lancet 387, 2026–2034 (2016). [PubMed: 27203778]

11. Shin'oka T, Imai Y, Ikada Y, Transplantation of a tissue-engineered pulmonary artery. N. Engl. J. Med. 344, 532–533 (2001). [PubMed: 11221621]
12. Naito Y, Imai Y, Shin'oka T, Kashiwagi J, Aoki M, Watanabe M, Matsumura G, Kosaka Y, Konuma T, Hibino N, Murata A, Miyake T, Kurosawa H, Successful clinical application of tissue-engineered graft for extracardiac Fontan operation. J. Thorac. Cardiovasc. Surg. 125, 419–420 (2003). [PubMed: 12579118]
13. Matsumura G, Hibino N, Ikada Y, Kurosawa H, Shin'oka T, Successful application of tissue engineered vascular autografts: Clinical experience. Biomaterials 13, 2303–2308 (2003).
14. Shin'oka T, Matsumura G, Hibino N, Naito Y, Watanabe M, Konuma T, Sakamoto T, Nagatsu M, Kurosawa H, Midterm clinical result of tissue-engineered vascular autografts seeded with autologous bone marrow cells. J. Thorac. Cardiovasc. Surg. 129, 1330–1338 (2005). [PubMed: 15942574]
15. Hibino N, McGillicuddy E, Matsumura G, Ichihara Y, Naito Y, Breuer C, Shinoka T, Late-term results of tissue-engineered vascular grafts in humans. J. Thorac. Cardiovasc. Surg. 139, 431–436.e2 (2010). [PubMed: 20106404]
16. Bockeria LA, Svanidze O, Kim A, Shatalov K, Total cavopulmonary connection with a new bioabsorbable vascular graft : First clinical experience. J. Thorac. Cardiovasc. Surg. 153, 1542–1550 (2017). [PubMed: 28314534]
17. Miller KS, Lee YU, Naito Y, Breuer CK, Humphrey JD, Computational model f the in vivo development of a tissue engineered vein from an implanted polymeric construct. J. Biomech. 47, 2080–2087 (2014). [PubMed: 24210474]
18. Miller KS, Khosravi R, Breuer CK, Humphrey JD, A hypothesis-driven parametric study of effects of polymeric scaffold properties on tissue engineered neovessel formation. Acta Biomater. 11, 283–294 (2015). [PubMed: 25288519]
19. Szafron JM, Khosravi R, Reinhardt J, Best CA, Bersi MR, Yi T, Breuer CK, Humphrey JD, Immuno-driven and mechano-mediated neotissue formation in tissue engineered vascular grafts. Ann. Biomed. Eng. 46, 1938–1350 (2018). [PubMed: 29987541]
20. Garg K, Pullen NA, Oskeritzian CA, Ryan JJ, Bowlin GL, Macrophage functional polarization (M1/M2) in response to varying fiber and pore dimensions of electrospun scaffolds. Biomaterials 34, 4439–4451 (2013). [PubMed: 23515178]
21. Sussman EM, Halpin MC, Muster J, Moon RT, Ratner BD, Porous implants modulate healing and induce shifts in local macrophage polarization in the foreign body reaction. Ann. Biomed. Eng. 42, 1508–1516 (2014). [PubMed: 24248559]
22. Brennan MP, Dardik A, Hibino N, Roh JD, Nelson GN, Papademitris X, Shinoka T, Breuer CK, Tissue engineered vascular grafts demonstrate evidence of growth and development when implanted in a juvenile animal model. Ann. Surg. 248, 370–377 (2008). [PubMed: 18791357]
23. Kurobe H, Maxfield MW, Naito Y, Cleary M, Stacy MR, Solomon D, Rocco KA, Tara S, Lee AY, Sinusas AJ, Snyder EL, Shinoka T, Breuer CK, Comparison of a closed system to a standard open technique for preparing tissue-engineered vascular grafts. Tissue Eng. Part C Methods 21, 88–93 (2015). [PubMed: 24866863]
24. Pepper VK, Clark ES, Best CA, Onwuka EA, Sugiura T, Heuer ED, Moko LE, Miyamoto S, Miyachi H, Berman DP, Cheatham SL, Chisolm JL, Shinoka T, Breuer CK, Cheatham JP, Intravascular ultrasound characterization of a tissue-engineered vascular graft in an ovine model. J. Cardiovasc. Transl. Res. 10, 128–138 (2017). [PubMed: 28097523]
25. Roh JD, Sawh-Martinez R, Brennan MP, Jay SM, Devine L, Rao DA, Yi T, Mirensky TL, Nalbandian A, Udelsman B, Hibino N, Shinoka T, Saltzman WM, Snyder E, Kyriakides TR, Pober JS, Breuer CK, Tissue-engineered vascular grafts transform into mature blood vessels via an inflammation-mediated process of vascular remodeling. Proc. Natl. Acad. Sci. U.S.A. 107, 4669–4674 (2010). [PubMed: 20207947]
26. Hibino N, Yi T, Duncan DR, Rathore A, Dean E, Naito Y, Dardik A, Kyriakides T, Madri J, Pober JS, Shinoka T, Breuer CK, A critical role for macrophages in neovessel formation and the

development of stenosis in tissue-engineered vascular grafts. FASEB J. 25, 4253–4263 (2011). [PubMed: 21865316]

27. Harrington JK, Chahboune H, Criscione JM, Li AY, Hibino N, Yi T, Villalona GA, Kobsa S, Meijas D, Duncan DR, Devine L, Papademetri X, Shin'oka T, Fahmy TM, Breuer CK, Determining the fate of seeded cells in venous tissue-engineered vascular grafts using serial MRI. FASEB J. 25, 4150–4161 (2011). [PubMed: 21846838]
28. Hibino N, Villalona G, Pietris N, Duncan DR, Schoffner A, Roh JD, Yi T, Dobrucki LW, Mejias D, Sawh-Martinez R, Harrington JK, Sinusas A, Krause DS, Kyriakides T, Saltzman WM, Pober JS, Shin'oka T, Breuer CK, Tissue-engineered vascular grafts form neovessels that arise from regeneration of the adjacent blood vessel. FASEB J. 25, 2731–2739 (2011). [PubMed: 21566209]
29. Duncan DR, Chen PY, Patterson JT, Lee YU, Hibino N, Cleary M, Naito Y, Yi T, Gilliland T, Kurobe H, Church SN, Shinoka T, Fahmy TM, Simons M, Breuer CK, TGFβR1 inhibition blocks the formation of stenosis in tissue-engineered vascular grafts. J. Am. Coll. Cardiol. 65, 512–514 (2015). [PubMed: 25660932]
30. Lee YU, de Dios Ruiz-Rosado J, Mahler N, Best CA, Tara S, Yi T, Shoji T, Sugiura T, Lee AY, Robledo-Avila F, Hibino N, Pober JS, Shinoka T, Partida-Sanchez S, Breuer CK, TGF-β receptor 1 inhibition prevents stenosis of tissue-engineered vascular grafts by reducing host mononuclear phagocyte activation. FASEB J. 30, 2627–2636 (2016). [PubMed: 27059717]
31. Tara S, Kurobe H, de Dios Ruiz Rosado J, Best CA, Shoji T, Mahler N, Yi T, Lee YU, Sugiura T, Hibino N, Partida-Sanchez S, Breuer CK, Shinoka T, Cilostazol, not aspirin, prevents stenosis of bioresorbable vascular grafts in a venous model. Arterioscler. Thromb. Vasc. Biol. 35, 2003–2010 (2015). [PubMed: 26183618]
32. Lee YU, Mahler N, Best CA, Tara S, Sugiura T, Lee AY, Yi T, Hibino N, Shinoka T, Breuer CK, Rational design of an improved tissue-engineered vascular graft: Determining the optimal cell dose and incubation time. Regen. Med. 11, 159–167 (2016). [PubMed: 26925512]
33. Ruiz-Rosado JD, Lee YU, Mahler N, Yi T, Robledo-Avila F, Martinez-Saucedo D, Lee AY, Shoji T, Heuer E, Yates AR, Pober JS, Shinoka T, Partida-Sanchez S, Breuer CK, Angiotensin II receptor I blockade prevents stenosis of tissue engineered vascular grafts. FASEB J. 32, 6822–6832 (2018).
34. L'Heureux N, Dusserre N, Konig G, Victor B, Keire P, Wight TN, Chronos NA, Kyles AE, Gregory CR, Hoyt G, Robbins RC, McAllister TN, Human tissue-engineered blood vessels for adult arterial revascularization. Nat. Med. 12, 361–365 (2006). [PubMed: 16491087]
35. Syedain ZH, Graham ML, Dunn TB, Brien TO, Johnson SL, Schumacher RJ, Tranquillo RT, A completely biological " off-the-shelf " arteriovenous graft that recellularizes in baboons. Sci. Transl. Med. 9, eaan4209 (2017). [PubMed: 29093182]
36. Quint C, Kondo Y, Manson RJ, Lawson JH, Dardik A, Niklason LE, Decellularized tissue-engineered blood vessel as an arterial conduit. Proc. Natl. Acad. Sci. U.S.A. 108, 9214–9219 (2011). [PubMed: 21571635]
37. Syedain ZH, Meier LA, Bjork JW, Lee A, Tranquillo RT, Implantable arterial grafts from human fibroblasts and fibrin using a multi-graft pulsed flow-stretch bioreactor with noninvasive strength monitoring. Biomaterials 32, 714–722 (2011). [PubMed: 20934214]
38. L'Heureux N, Paquet S, Labbe R, Germain L, Auger FA, A completely biological tissue-engineered human blood vessel. FASEB J. 12, 47–56 (1998). [PubMed: 9438410]
39. Niklason LE, Gao J, Abbott WM, Hirschi KK, Houser S, Marini R, Langer R, Functional arteries grown in vitro. Science 284, 489–493 (1999). [PubMed: 10205057]
40. Dahl SLM, Kypson AP, Lawson JH, Blum JL, Strader JT, Li Y, Manson RJ, Tente WE, DiBernardo L, Hensley MT, Carter R, Williams TP, Prichard HL, Dey MS, Begelman KG, Niklason LE, Readily available tissue-engineered vascular grafts. Sci. Transl. Med. 3, 68ra9 (2011).
41. Hoerstrup SP, Cummings I, Lachat M, Schoen FJ, Jenni R, Leschka S, Neuenschwander S, Schmidt D, Mol A, Günter C, Gössi M, Genoni M, Zund G, Functional growth in tissue-engineered living, vascular grafts: Follow-up at 100 weeks in a large animal model. Circulation 114, 159–167 (2006).

42. Cummings I, George S, Kelm J, Schmidt D, Emmert MY, Weber B, Zünd G, Hoerstrup SP, Tissue-engineered vascular graft remodeling in a growing lamb model: Expression of matrix metalloproteinases. Eur. J. Cardiothorac. Surg. 41, 167–172 (2012). [PubMed: 21530291]
43. Brugmans M, Serrero A, Cox M, Svanidze O, Schoen FJ, Morphology and mechanisms of a novel absorbable polymeric conduit in the pulmonary circulation of sheep. Cardiovasc. Pathol. 38, 31–38 (2019). [PubMed: 30428421]
44. C. A. Best, Szafron JM, Rocco KA, Zbinden J, Dean EW, Maxfield MW, Kurobe H, Tara S, Bagi PS, Udelsman BV, Khosravi R, Yi T, Shinoka T, Humphrey JD, Breuer CK, Differential outcomes of venous and arterial tissue engineered vascular grafts highlight the importance of coupling long-term implantation studies with computational modeling. Acta Biomater. 94, 183–194 (2019). [PubMed: 31200116]
45. Stylianopoulos T, Bashur CA, Goldstein AS, Guelcher SA, Barocas VH, Computational predictions of the tensile properties of electrospun fibre meshes: Effect of fibre diameter and fibre orientation. J. Mech. Behav. Biomed. Mater. 1, 326–335 (2008). [PubMed: 19627797]
46. Harrison S, Tamimi E, Uhlorn J, Leach T, Vande Geest JP, Computationally optimizing the compliance of a biopolymer based tissue engineered vascular graft. J. Biomech. Eng. 138, 014505 (2016).
47. Gronau G, Krishnaji ST, Kinahan ME, Giesa T, Wong JY, Kaplan DL, Buehler MJ, A review of combined experimental and computational procedures for assessing biopolymer structure-process-property relationships. Biomaterials 33, 8240–8255 (2012). [PubMed: 22938765]
48. Niklason LE, Yeh AT, Calle EA, Bai Y, Valentín A, Humphrey JD, Enabling tools for engineering collagenous tissues integrating bioreactors, intravital imaging, and biomechanical modeling. Proc. Natl. Acad. Sci. U.S.A. 107, 3335–3339 (2010). [PubMed: 19955446]
49. Zahedmanesh H, Lally CA, A multiscale mechanobiological modelling framework using agent-based models and finite element analysis: Application to vascular tissue engineering. Biomech. Model. Mechanobiol. 11, 363–377 (2012). [PubMed: 21626394]
50. Gade PS, Lee K, Pfaff BN, Wang Y, Robertson AM, Degradation and erosion mechanisms of bioresorbable porous acellular vascular grafts: An in vitro investigation. J. R. Soc. Interface 14, 20170102 (2017). [PubMed: 28701504]
51. Szafron JM, Ramachandra AB, Breuer CK, Marsden AL, Humphrey JD, Optimization of tissue-engineered vascular graft design using computational modeling. Tissue Eng. Part C Methods 10, 561–570 (2019).
52. Emmert MY, Schmitt BA, Loerakker S, Sanders B, Spriestersbach H, Fioretta ES, Bruder L, Brakmann K, Motta SE, Lintas V, Dijkman PE, Frese L, Berger F, Baaijens FPT, Hoerstrup SP, Computational modeling guides tissue-engineered heart valve design for long-term in vivo performance in a translational sheep model. Sci. Transl. Med. 10, eaan4587 (2018). [PubMed: 29743347]
53. Ramachandra AB, Sankaran S, Humphrey JD, Marsden AL, Computational simulation of the adaptive capacity of vein grafts in response to increased pressure. J. Biomech. Eng. 137, 031009 (2015).
54. Khosravi R, Miller KS, Best CA, Shih YC, Lee YU, Yi T, Shinoka T, Breuer CK, Humphrey JD, Biomechanical diversity despite mechanobiological stability in tissue engineered vascular grafts two years post-implantation. Tissue Eng. Part A 21, 1529–1538 (2015). [PubMed: 25710791]
55. Humphrey JD, Rajagopal KR, A constrained mixture model for arterial adaptations to a sustained step change in blood flow. Biomech. Model. Mechanobiol. 2, 109–126 (2003). [PubMed: 14586812]
56. Humphrey JD, Vascular adaptation and mechanical homeostasis at tissue, cellular, and sub-cellular levels. Cell Biochem. Biophys. 50, 53–78 (2008). [PubMed: 18209957]
57. Sugiura T, Matsumura G, Miyamoto S, Miyachi H, Breuer CK, Shinoka T, Tissue-engineered vascular grafts in children with congenital heart disease: Intermediate term follow-up. Semin. Thorac. Cardiovasc. Surg. 30, 175–179 (2018). [PubMed: 29427773]
58. Humphrey JD, Rajagopal KR, A constrained mixture model for growth and remodeling of soft tissues. Math. Models Methods Appl. Sci. 12, 407–430 (2002).

59. Baek S, Rajagopal KR, Humphrey JD, A theoretical model of enlarging intracranial fusiform aneurysms. J. Biomech. Eng. 128, 142–149 (2006). [PubMed: 16532628]
60. Valentin A, Cardamone L, Baek S, Humphrey JD, Complementary vasoactivity and matrix remodelling in arterial adaptations to altered flow and pressure. J. R. Soc. Interface 6, 293–306 (2009). [PubMed: 18647735]
61. Ramachandra AB, Humphrey JD, Marsden AL, Gradual loading ameliorates maladaptation in computational simulations of vein graft growth and remodelling. J. R. Soc. Interface 14, 20160995 (2017). [PubMed: 28566510]
62. Naito Y, Williams-Fritze M, Duncan DR, Church SN, Hibino N, Madri JA, Humphrey JD, Shinoka T, Breuer CK, Characterization of the natural history of extracellular matrix production in tissue-engineered vascular grafts during neovessel formation. Cells Tissues Organs 195, 60–72 (2012). [PubMed: 21996715]
63. Naito Y, Lee YU, Yi T, Church SN, Solomon D, Humphrey JD, Shinoka T, Breuer CK, Beyond burst pressure: Initial evaluation of the natural history of the biaxial mechanical properties of tissue-engineered vascular grafts in the venous circulation using a murine model. Tissue Eng. Part A 20, 346–355 (2014). [PubMed: 23957852]
64. Verification and Validation 40 Subcommittee, Assessing credibility of computational modeling through verification and validation: Application to medical devices. Am. Soc. Mech. Eng. (2018).
65. Hibino N, Nalbandian A, Devine L, Martinez RS, McGillicuddy E, Yi T, Karandish S, Ortolano GA, Shin'oka T, Snyder E, Breuer CK, Comparison of human bone marrow mononuclear cell isolation methods for creating tissue-engineered vascular grafts: Novel filter system versus traditional density centrifugation method. Tissue Eng. Part C Methods 17, 993–998 (2011). [PubMed: 21609305]
66. Humphrey JD, Kang T, Sakarda P, Anjanappa M, Computer-aided vascular experimentation: A new electromechanical test system. Ann. Biomed. Eng. 21, 33–43 (1993). [PubMed: 8434818]
67. Audet C, Dennis JE Jr., Mesh adaptive direct search algorithms for constrained optimization. SIAM J. Optim. 17, 188–217 (2006).
68. Wilson JS, Baek S, Humphrey JD, Importance of initial aortic properties on the evolving regional anisotropy, stiffness and wall thickness of human abdominal aortic aneurysms. J. R. Soc. Interface 9, 2047–2058 (2012). [PubMed: 22491975]
69. Wilson JS, Baek S, Humphrey JD, Parametric study of effects of collagen turnover on the natural history of abdominal aortic aneurysms. Proc. R. Soc. A 469, 20120556 (2013). [PubMed: 23633905]
70. Cyron CJ, Wilson JS, Humphrey JD, Mechanobiological stability: A new paradigm to understand the enlargement of aneurysms? J. R. Soc. Interface 11, 20140680 (2014). [PubMed: 25209402]
71. Valentin A, Humphrey JD, Evaluation of fundamental hypotheses underlying constrained mixture models of arterial growth and remodelling. Philos. Trans. R. Soc. A 367, 3585–3606 (2009).
72. Valentín A, Humphrey JD, Parameter sensitivity study of a constrained mixture model of arterial growth and remodeling. J. Biomech. Eng. 10, 101006 (2009).

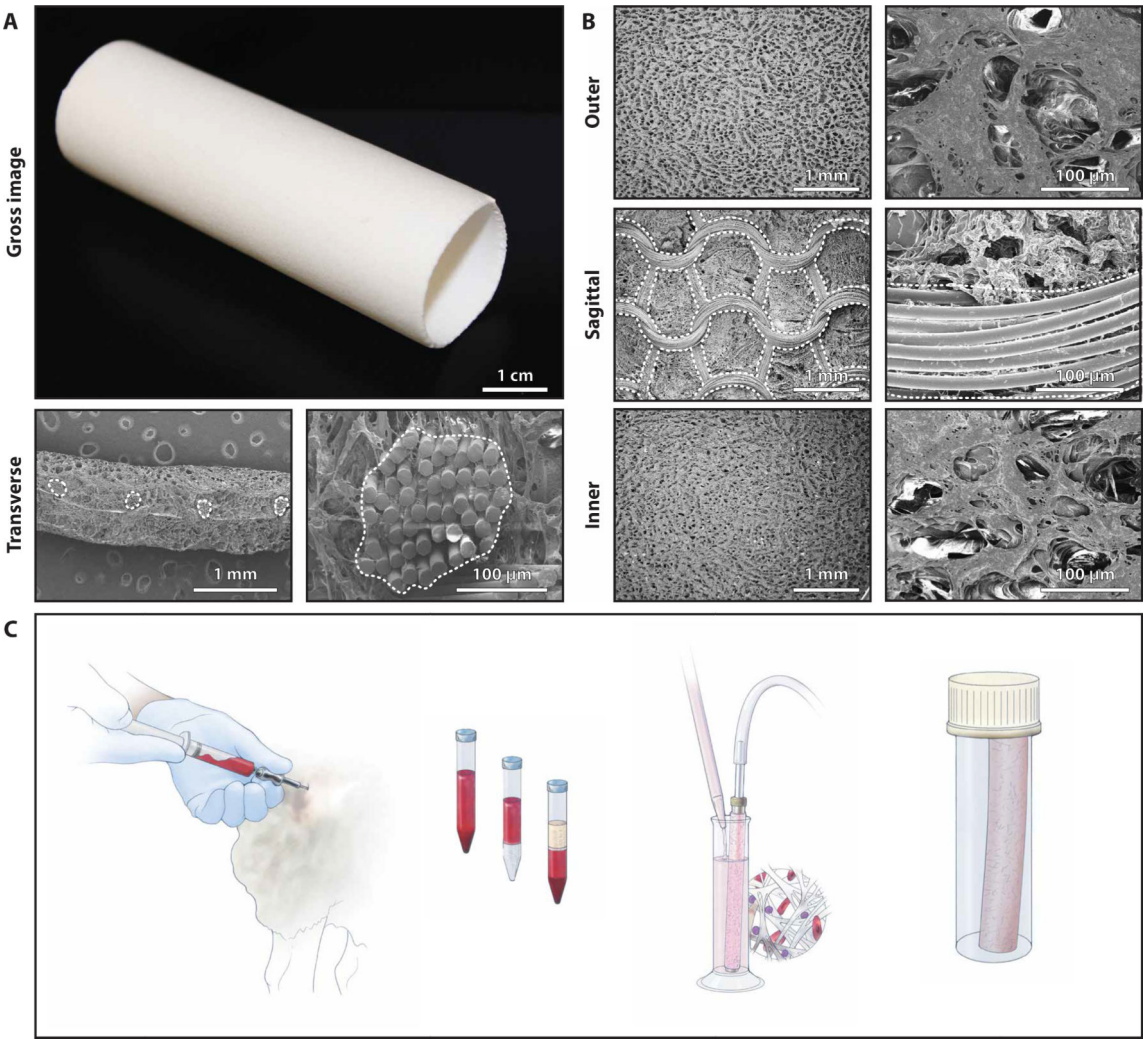

Fig. 1. Scaffold characterization and assembly of the TEVG.

(**A**) Gross image of a tubular scaffold. Low- and high-magnification transverse SEM images of the scaffold show the PGA fiber bundles, outlined in white. (**B**) Low-magnification (left) and high-magnification (right) SEM images of the scaffold showing the porous inner and outer surfaces, the middle layer, and the PGA fibers (when dividing the wall sagittally). (**C**) Schematic drawing demonstrating the method for assembling the TEVG. Briefly, whole bone marrow is aspirated from the iliac crest and mononuclear cells are enriched via density gradient centrifugation and vacuum-seeded on the tubular scaffold, then incubated for 2 hours before implantation as a vascular graft.

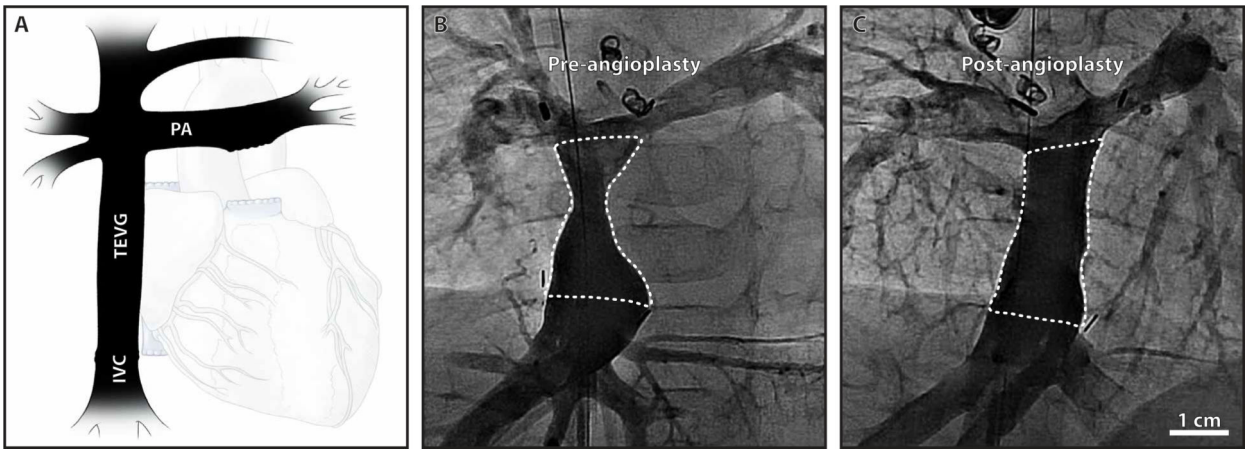

Fig. 2. Clinical performance of the TEVG.

(**A**) Schematic drawing of the Fontan anatomy as it would appear during a routine angiogram. Representative angiograms (anteroposterior view) of the TEVG obtained (**B**) before angioplasty and (**C**) after angioplasty in a case of critical stenosis. The TEVG is outlined with a dotted white line.

A Evolving mass turnover [due to production $m^{\alpha}(\tau)$ and removal $q^{\alpha}(s,\tau)$]

$$\rho(s)\ \text{(graft mass)} = \rho^{p}(s)\ \text{(polmyer mass)} + \rho^{i}(s)\ \text{(immuno-mediated mass)} + \rho^{\mathrm{m}}(s)\ \text{(mechano-mediated mass)}$$

with $\rho^{\alpha}(s) = \rho^{\alpha}(0)Q^{\alpha}(s) + \int_0^s m^{\alpha}(\tau)q^{\alpha}(s,\tau)d\tau$, for $Q^{\alpha}(s) \in [0,1]$, $\alpha = p,\ i,$ or m

where $m^{\mathrm{i}}(\tau) = f\left(\delta, \beta, K_{\mathrm{h}}^{\mathrm{i}}\right)$ and $q^{\mathrm{i}}(s,\tau) = g(K_{\mathrm{h}}^{\mathrm{i}}, K_{\mathrm{max}}^{\mathrm{i}})$ for immuno-mediated constituents

and $m^{\mathrm{m}}(\tau) = \hat{f}(\Delta t_{\theta}, \Delta\tau_{\mathrm{w}})$ and $q^{\mathrm{m}}(\mathrm{s},\tau) = \hat{g}(\Delta t_{\theta})$ for mechano-mediated constituents

B Inflammatory parameters (inputs)

Parameters	Inflammatory response effects	Values	Units
δ	Onset and duration of inflammatory response	[0.075, 0.15, 0.30, 0.50, 0.70]	1/days
β	shape and skew of inflammatory response	[1, 1.5, 2.0, 3.0, 4.0]	(-)
$K_{\mathrm{h}}^{\mathrm{i}}$	Rate of inflammatory cell/matrix production and degradation	[0.5, 1.0, 2.0, 4.0, 8.0]	(-)
$K_{\mathrm{max}}^{\mathrm{i}}$	Rate of inflammatory cell/matrix degradation	[5, 10, 20, 40, 80]	(-)

Simulated TEVG responses (outputs)

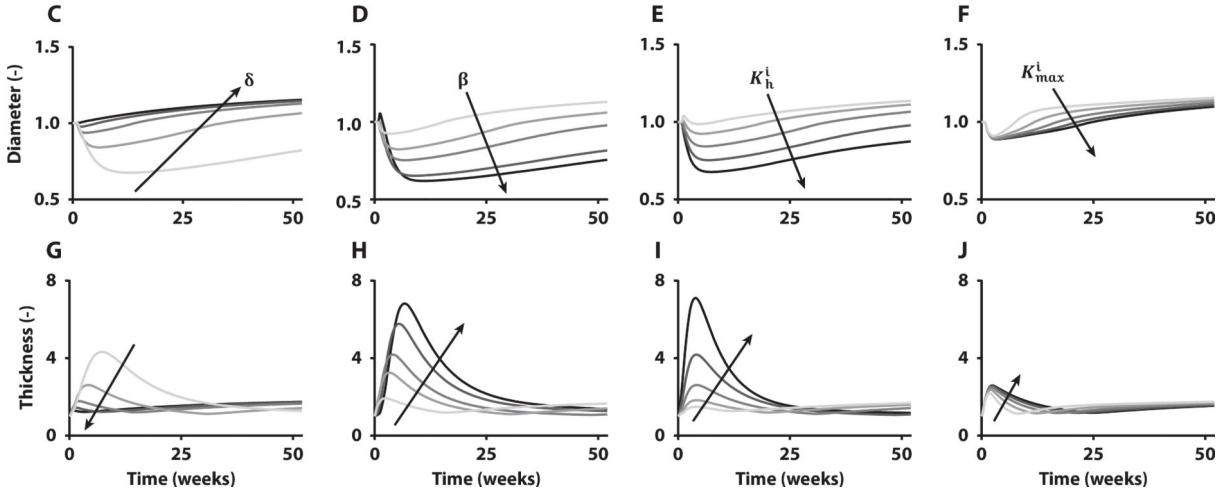

Fig. 3. Computational modeling predicts spontaneously reversible TEVG stenosis.

(**A**) Key equation within the overall computational model of TEVG development that accounts for changes in overall graft mass via changes in the rates of production m^{α} and removal q^{α} of different constituents α, each of which can depend on the inflammatory burden (superscript i), due to the foreign body response, and/or mechanobiological responses (superscript m), due to deviations Δ in circumferential wall stress t_{θ} and luminal wall shear stress τ_{w} from homeostatic values. Here, $f,\hat{f}$ and $g,\hat{g}$ denote general functions, given in the Supplementary Materials. (**B**) Table of four key model parameters and possible ranges identified from previous experiments in immunocompetent and immunocompromised mice to bound the possible inflammation-driven process of neovessel formation. (**C** to **J**) Parametric studies for these four key parameters: δ modulates the onset and duration of the inflammatory response, β dictates the shape and skew of the inflammatory time course, $K_{\mathrm{h}}^{\mathrm{i}}$ controls the peak rates of inflammatory neotissue production and degradation, and $K_{\mathrm{max}}^{\mathrm{i}}$

scales inflammatory effects on neotissue degradation. Each plot focuses on the early evolution, up to 52 weeks after implantation, of normalized luminal diameter (top row) and wall thickness (bottom row) for variations in δ, β, κ_h^i, and κ_{max}^i, with arrows showing the direction of increasing values given in the table above.

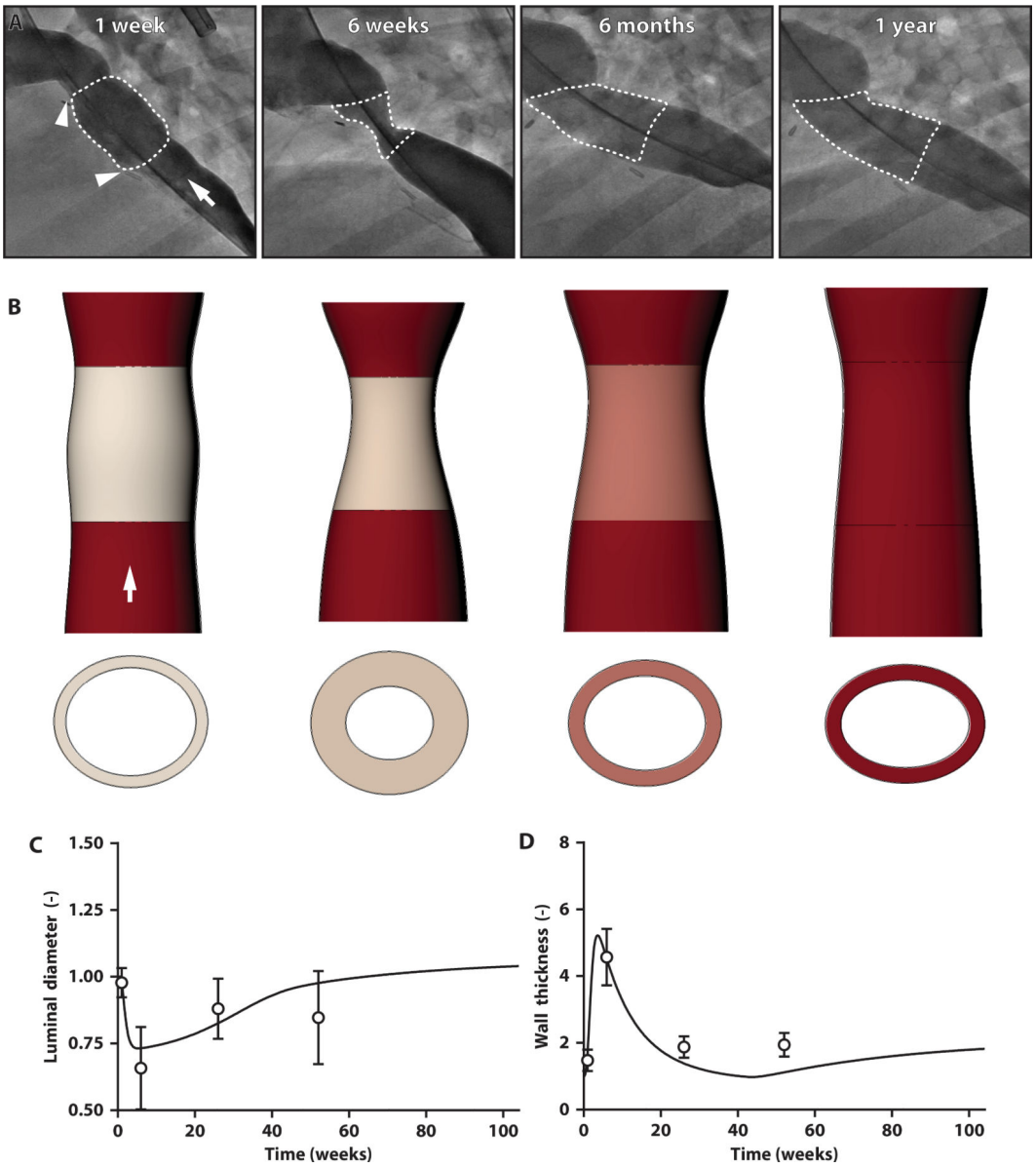

Fig. 4. TEVG stenosis spontaneously reverses in an ovine model.

(**A**) Serial angiographic images of a representative ovine TEVG 1 week, 6 weeks, 6 months, and 1 year after implantation. Anastomoses are identified with white arrowheads, and the TEVG is identified by a white dotted outline. White arrow indicates direction of blood flow. (**B**) Image reconstructions of serial IVUS and angiographic measurements of luminal area, wall thickness, and length of the TEVG, confirming the development of stenosis at 6 weeks but spontaneous resolution by 6 months after implantation. White arrow indicates direction of blood flow. When based on lamb data, the model simulations (solid lines) for the midgraft (**C**) luminal diameter and (**D**) wall thickness fit well the hydraulic diameters calculated from the IVUS measurements (symbols) over the 1-year study. Ovine IVUS measurements are represented as means ± SD (n = 22 at 1 week, n = 22 at 6 weeks, n = 20 at 6 months, n = 15 at 1 year).

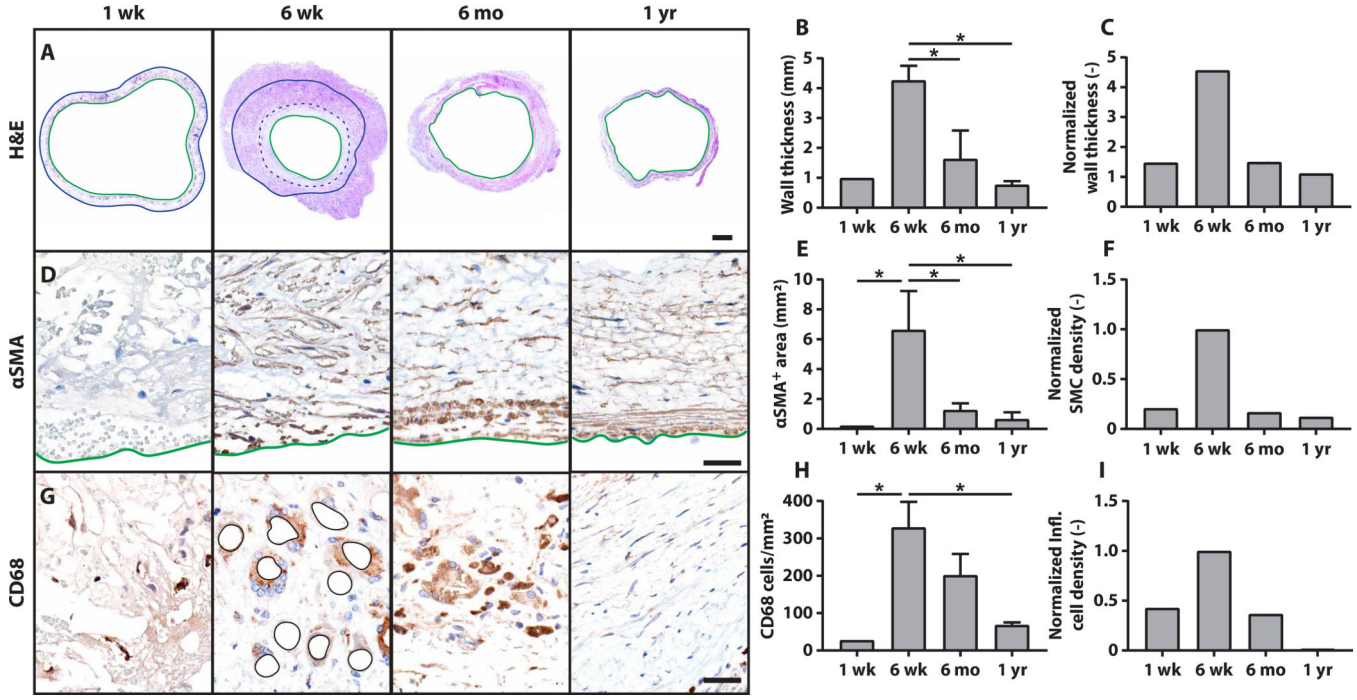

Fig. 5. Stenosis arises from excessive inflammation-driven neotissue formation.

(**A**) Low-magnification images of hematoxylin and eosin (H&E) staining confirm findings from the in vivo imaging that stenosis results from the formation of neotissue on the inner surface of the scaffold and within the wall, causing wall thickening and luminal narrowing. Green solid lines indicate the neovessel lumen, blue dotted lines indicate luminal neotissue formation, and solid blue lines indicate the abluminal surface of the scaffold. Scale bar, 2.0 mm. (**B**) Quantitative histological analysis of wall thickness and (**C**) model simulations of TEVG wall thickness over time (one-way ANOVA with Tukey's post hoc multiple comparisons test, $\alpha = 0.05$, $^*P < 0.05$). (**D**) Staining for αSMA expression. Solid green lines indicate the luminal border of the neovessel. Scale bar, 40 μm. (**E**) Quantifications of αSMA$^+$ area within the vascular neotissue over time and (**F**) model predictions of smooth muscle cell density (one-way ANOVA with Tukey's post hoc multiple comparisons test, $\alpha = 0.05$, $^*P < 0.05$). (**G**) Staining for CD68$^+$ macrophages and (**H**) quantification (one-way ANOVA with Tukey's post hoc multiple comparisons test, $\alpha = 0.05$, $^*P < 0.05$). Remaining scaffold polymer at 6 weeks is outlined in black. (**I**) Computational model predictions of inflammatory cell density. Plotted data represent means ± SEM ($n = 1$ at 1 week, $n = 2$ at 6 weeks, $n = 4$ at 6 months, $n = 2$ at 1 year).

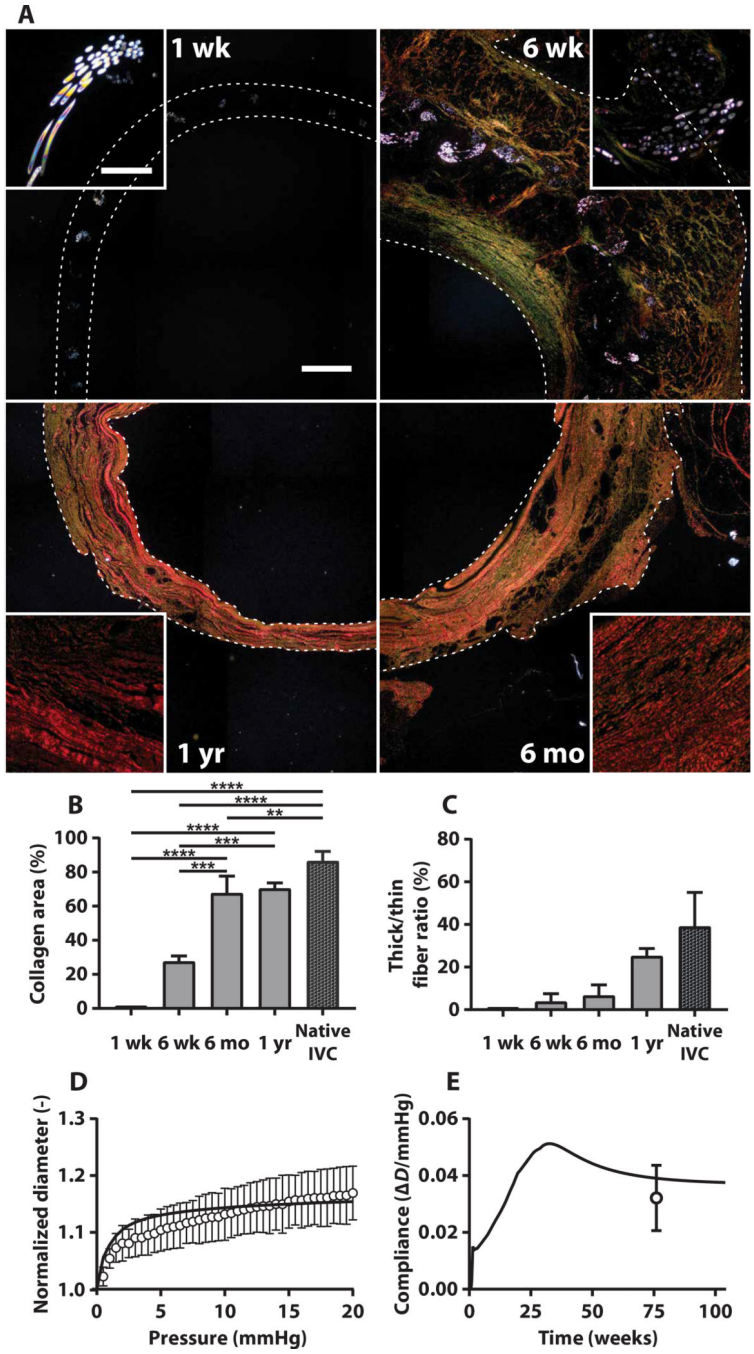

Fig. 6. Extracellular matrix production and remodeling, scaffold degradation, and mechanical properties of the neovessel are consistent with model predictions.

(**A**) Polarized light images (25×) of PSR-stained transverse sections of the mid-TEVG 1 week, 6 weeks, 6 months, and 1 year after implantation (clockwise). Scale bar, 1.0 mm. White insets highlight 200× polarized light images of the birefringent polymeric scaffold apparent at 1 and 6 weeks, which is subsequently replaced by increasingly thick and aligned collagen fibers at 6 months and 1 year. Scale bar, 40 μm. (**B**) Quantification of total collagen area fraction from the PSR stain over time compared to the native IVC (one-way ANOVA

with Tukey's multiple comparisons test, $\alpha = 0.05$, $^{**}P < 0.005$, $^{***}P < 0.0005$, and $^{****}P < 0.0001$; plot represents means ± SEM; $n = 1$ at 1 week, $n = 2$ at 6 weeks, $n = 4$ at 6 months, $n = 2$ at 1 year). (**C**) Ratio of thick-to-thin collagen fibers in the TEVG over time compared to the native IVC (means ± SEM). $n = 1$ at 1 week, $n = 2$ at 6 weeks, $n = 4$ at 6 months, $n = 2$ at 1 year. (**D**) Experimental measurements of the mechanical behavior of the TEVG in response to in vitro pressurization after 1.5 years of development in vivo (symbols represent means ± SD); predicted values from the computational model are shown with a solid line. (**E**) Predicted graft compliance over 2 to 3 mmHg through 2 years of simulated neovessel development (solid line); the experimentally measured compliance at 18 months is shown by symbol representing mean ± SD.

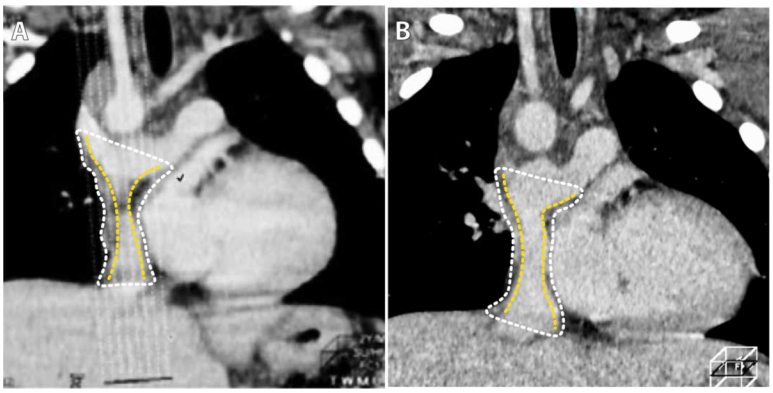

Fig. 7. Potential clinical case of reversible TEVG stenosis.

(**A**) CT images of the TEVG (outer wall outlined with white dots and lumen outlined with yellow dots) from patient 13 from the Japanese trial demonstrating wall thickening and luminal narrowing that presented during the first year after implantation and (**B**) resolved over the course of several months after treatment with oral anticoagulation (15).